

DRAFT VERSION SEPTEMBER 4, 2022

Typeset using L<sup>A</sup>T<sub>E</sub>X preprint style in AASTeX63

## Direct radio discovery of a cold brown dwarf

H. K. VEDANTHAM,<sup>1,2</sup> J. R. CALLINGHAM,<sup>3,1</sup> T. W. SHIMWELL,<sup>1,3</sup> T. DUPUY,<sup>4,5</sup>  
WILLIAM M. J. BEST,<sup>6,7</sup> MICHAEL C. LIU,<sup>7,8</sup> ZHOUIAN ZHANG,<sup>8</sup> K. DE,<sup>9</sup> L. LAMY,<sup>10</sup> P. ZARKA,<sup>10</sup>  
H. J. A. RÖTTGERING,<sup>3</sup> AND A. SHULEVSKI<sup>3</sup>

<sup>1</sup>*ASTRON, Netherlands Institute for Radio Astronomy, Oude Hoogeveensedijk 4, 7991PD, Dwingeloo, The Netherlands*

<sup>2</sup>*Kapteyn Astronomical Institute, University of Groningen, The Netherlands*

<sup>3</sup>*Leiden Observatory, Leiden University, PO Box 9513, 2300 RA Leiden, The Netherlands*

<sup>4</sup>*Institute for Astronomy, University of Edinburgh, Blackford Hill, Edinburgh, EH9 3HJ, United Kingdom*

<sup>5</sup>*Gemini Observatory, Northern Operations Center, 670 N. A'ohoku Place, Hilo, HI 96720, USA*

<sup>6</sup>*University of Texas at Austin, Department of Astronomy, 2515 Speedway C1400, Austin, TX 78712, USA*

<sup>7</sup>*Visiting Astronomer at the Infrared Telescope Facility, which is operated by the University of Hawaii under contract 80HGTR19D0030 with the National Aeronautics and Space Administration.*

<sup>8</sup>*Institute for Astronomy, University of Hawai'i, 2680 Woodlawn Drive, Honolulu, HI 96822*

<sup>9</sup>*Cahill center for astronomy and astrophysics, California Institute of Technology, 1200 E California Blvd. Pasadena, CA, 91125*

<sup>10</sup>*LESIA, CNRS – Observatoire de Paris, PSL 92190, Meudon, France*

(Received; Revised; Accepted)

Submitted to ApJL

### ABSTRACT

Magnetospheric processes seen in gas-giants such as aurorae and circularly-polarized cyclotron maser radio emission have been detected from some brown dwarfs. However, previous radio observations targeted known brown dwarfs discovered via their infrared emission. Here we report the discovery of BDR 1750+3809, a circularly polarized radio source detected around 144 MHz with the LOFAR telescope. Follow-up near-infrared photometry and spectroscopy show that BDR 1750+3809 is a cold methane dwarf of spectral type  $T6.5 \pm 1$  at a distance of  $65_{-8}^{+9}$  pc. The quasi-quietest radio spectral luminosity of BDR 1750+3809 is  $\approx 5 \times 10^{15} \text{ erg s}^{-1} \text{ Hz}^{-1}$  which is over two orders of magnitude larger than that of the known population of comparable spectral type. This could be due to a preferential geometric alignment or an electrodynamic interaction with a close companion. In addition, as the emission is expected to occur close to the electron gyro-frequency, the magnetic field strength at the emitter site in BDR 1750+3809 is  $B \gtrsim 25 \text{ G}$ , which is comparable to planetary-scale magnetic fields. Our discovery suggests that low-frequency radio surveys can be employed to discover sub-stellar objects that are too cold to be detected in infrared surveys.

Corresponding author: H. K. Vedantham  
vedantham@astron.nl

*Keywords:* brown dwarfs — planets and satellites: aurorae — stars: magnetic field — planets and satellites: magnetic fields

## 1. INTRODUCTION

The generation and dissipation of magnetic flux in stars and planets is pivotal in driving violent stellar activity and determining the space plasma environment around exoplanets respectively (Schrijver & Zwaan 2008; Schwenn 2006). On cool objects where Zeeman splitting observations are difficult (later than type M typically), observation of cyclotron emission, that falls in the radio band, is the only known technique to directly measure the strength and topology of the objects’ magnetic fields.

Brown dwarfs (BD), with masses between that of stars and planets, display optical aurorae (Hallinan et al. 2015) and the associated auroral radio emission (Hallinan et al. 2015; Kao et al. 2018; Pineda et al. 2017; Nichols et al. 2012) powered by the electron cyclotron maser instability (Hallinan et al. 2008; Wu & Lee 1979; Treumann 2006). In addition, because there appears to be no clear demarcation between the atmospheres and magnetospheres of the smallest coldest brown dwarfs and the largest planets (Deeg & Belmonte 2018), radio observations at the end of the BD sequence are expected to provide a tantalizing glimpse into magnetospheric properties of exoplanets (Kao et al. 2018, 2019).

Christensen et al. (2009) have argued that the magnetic fields of planets, brown dwarfs, and low-mass stars of sufficiently rapid rotation are dipolar and that the field strength scales with the heat-flux from the bodies’ interior. The simplicity and universality of this law is a giant leap in modeling exoplanet atmospheres and habitability. The law can be tested at the low-mass end by measuring the magnetic fields of a sample of cold brown dwarfs and exoplanets via radio observations of their cyclotron emission (Kao et al. 2016, 2018).<sup>1</sup>

Since their discovery as radio-emitters (Berger et al. 2001), radio surveys of known BDs have primarily been carried out at gigahertz frequencies that can only detect cyclotron emission from objects with kG-level magnetic fields (see the compilation of Pineda et al. 2017; Williams 2018, Chapter 28). Observations at much lower frequencies that probe ‘planetary scale’ magnetic fields (few to tens of Gauss) are necessary to test the scaling law in the exoplanet-regime. Low frequency observations are now being carried out thanks to the advent of sensitive metre-wave telescopes such as LOFAR (van Haarlem et al. 2013), and the wide-area surveys they facilitate such as the LoTSS survey (Shimwell et al. 2017, 2019). Low-frequency searches have so far been unsuccessful (Bastian et al. 2000; Lazio et al. 2004; Hallinan et al. 2013; Burningham et al. 2016; Lynch et al. 2017b; Lenc et al. 2018).

Searching for circularly polarized radio sources has proved to be a powerful technique to identify coherent stellar radio emission (Lynch et al. 2017a; Vedantham et al. 2020; Callingham et al. 2020). There are three known types of radio emitter with high circularly polarized (CP) fraction: (a) stars, (b) brown dwarfs and planets, and (c) pulsars. Lack of an optical counterpart to a CP source generally rules out a stellar association. We are currently following up such sources in the LoTSS survey (Shimwell et al. 2017, 2019) data with NIR photometry and radio pulsation search to distinguish between the remaining two options. Here we report our first discovery from this effort— BDR 1750+3809. We will leave the overall counts and population statistics of unassociated

<sup>1</sup> The emission happens at the cyclotron frequency,  $\nu_c \approx 2.8(B/\text{Gauss})$  MHz or its second harmonic (Melrose & Dulk 1982), where  $B$  is the magnetic field strength.

CP sources for future work, save mention that BDR 1750+3809 stood out due to its high CP fraction (see §2.1 below) and that follow-up near-infrared photometric observations show the object to be a cold brown dwarf (see §2.2 below).

BDR 1750+3809 is the first radio-selected substellar object, which demonstrates that such objects can be directly discovered in a sensitive wide-area radio surveys. Because, the intensity of magnetospheric radio emission, that is non-thermal in nature, need not have a one-to-one scaling with the object’s infrared luminosity, which is thermal in nature, BDR 1750+3809’s discovery also shows that ongoing low-frequency radio surveys could discover objects that are too cold and/or distant to be discovered and studied via their infrared emission.

## 2. DISCOVERY AND FOLLOW-UP

### 2.1. *Radio properties*

BDR 1750+3809 was discovered as a radio source in an 8-hr LOFAR exposure between 120 and 167 MHz with a high average CP fraction of  $\approx 96^{+4}_{-20}\%$ . The field containing BDR 1750+3809 was covered by two partially-overlapping LoTSS survey pointings, which were observed approximately six months apart in 2018. The radio source was only detected in one exposure (Fig. 1). Separately, we obtained another LOFAR exposure centered on BDR 1750+3809 in January 2020. We re-detected the source in total intensity at low significance ( $\approx 4\sigma$ ), but not in circular polarization. Forced CP photometry yields a polarized fraction of  $12 \pm 16\%$ . The radio source has not been detected previously, including in the first-epoch of the ongoing VLA Sky Survey at 2 – 4 GHz (image noise of  $\approx 0.1$  mJy; Lacy et al. 2020). Further details of radio data processing are given in Appendix A.

### 2.2. *Identification as a cold brown dwarf*

We searched publicly available optical and NIR archives for an association with the radio source. The source has no counterpart in the Pan-STARRS (Chambers et al. 2016), 2MASS (Skrutskie et al. 2006) or AllWISE (Cutri & et al. 2013) survey catalogs. We found a faint ( $6\sigma$  level) *J*-band detection (Fig. 2) positionally coincident with BDR 1750+3809 in the UKIRT Hemisphere Survey (UHSDR1; Dye et al. 2018).

To confirm the UKIRT detection and constrain the NIR colors, we obtained a *Ks* band image of the source with the Wide-field Infrared Camera (WIRC; Wilson et al. 2003) on the Palomar 200-inch telescope. The data were reduced and stacked using a custom data reduction pipeline described in De et al. (2020). With an effective exposure of 10 min, we did not secure a detection at the location of the UKIRT *J*-band source (Fig. 2). However, the  $\approx 6$  year baseline between the two 200-inch and UKIRT exposures, and the unknown proper motion of BDR 1750+3809, meant that we could not be certain if sub-threshold (low significance) detections in the *Ks*-band image could be associated.

We obtained time for *J*– and *Y*-band photometry on the Gemini-North telescope (proposal id DT-2019B-014). Because the workhorse imager, NIRI (Hodapp et al. 2003), was unavailable at that time, we obtained imaging exposures through the acquisition keyhole of the GNIRS spectrometer (Elias et al. 2006). This option yields a sensitivity comparable to that of NIRI but with a small field of view. The observing conditions did not permit the transfer of calibration solutions from photometric standards. We therefore tied our photometry to the nearby star 2MASS J17500008+3809276 (Star A hereafter; see appendix for further details).

We detected the counterpart to BDR 1750+3809 in both *J* and *Y* bands in the GNIRS keyhole images (Fig. 2). We used the known position of the source from the 2019-10-19 GNIRS exposures

to search for a sub-threshold detection in the  $Ks$  band data from 2019-09-07. A forced photometric extraction yielded a faint  $3\sigma$  detection.

We also found a  $\approx 5\sigma$  detection in the  $W1$  and  $W2$  channels of the unWISE catalog (Schlafly et al. 2019) that is an un-blurred co-addition of all available WISE exposures. Bulk of the WISE exposures of the field around BDR 1750+3809, were taken in 2010. The WISE detections are consistent with the proper-motion corrected position of BDR 1750+3809, (see §2.4 below) within errors. The NIR colors ( $Y - J$ ,  $J - H$  and  $J - W2$  for e.g.; see also Fig. 8) identify the object as a cold brown dwarf of spectral class T.

### 2.3. Spectral type & Distance

T-dwarfs are characterized by the presence of methane in their atmosphere (Fegley & Lodders 1996; Kirkpatrick et al. 1999) due to their low surface temperatures that range from a few hundred to  $\sim 1000$  K (Nakajima et al. 2004). To confirm the presence of atmospheric methane, we obtained further exposures using the NIRI instrument on the Gemini North telescope in  $H$ -band and the  $\text{CH}_4s$  band to perform ‘methane-imaging’, which is a reliable technique for discovery and spectral typing of cool BDs (Rosenthal et al. 1996; Tinney et al. 2005). We detected BDR 1750+3809 in both filters at high significance (Fig. 2). Based on the observed  $H - \text{CH}_4s$  colors of the object and the relationship of Liu et al. (2008, their Eqn. 2 and Fig 4), we estimate a spectral type of  $T7.5 \pm 1.5$ , confirming that BDR 1750+3809 is at the end of the T-dwarf sequence.

Separately, We obtained low-resolution ( $R \approx 100$ ) spectrum of BDR 1750+3809 on 2020 October 4 UT using the near-IR spectrograph Spex (Rayner et al. 2003) on NASA’s Infrared Telescope Facility (IRTF) located on Maunakea, Hawaii. Figure 3 shows the reduced spectrum of BDR 1750+3809. While the S/N is low ( $\approx 6$  per pixel in the  $J$ -band peak), the spectrum clearly shows the strong water and methane absorption bands that are the hallmarks of late-T dwarfs. We classified BDR 1750+3809 from the system of five spectral indices established by Burgasser et al. (2006), resulting in a spectral type of  $T6.2 \pm 1.2$ . We also visually classified BDR 1750+3809 by comparing with IRTF/Spex spectra of the late-T standards from Burgasser et al. (2006), finding a type of T7. Considering both the index and visual types, we adopt a final type of  $T6.5 \pm 1.0$ .

All measurements of flux-density and position estimates are summarized in Table 1 for quick reference, while the Appendix provides further details of the observational setup and data processing.

### 2.4. Distance and Proper motion

We placed BDR 1750+3809 on the  $J$  versus  $J - W2$  color-magnitude relationship of cold methane dwarfs from Leggett et al. (2017) (see Fig. 9) to find a distance of  $d = 70_{-35}^{+25}$  pc. We estimated a more accurate photometric distance to BDR 1750+3809 using the spectral type-absolute magnitude relation from Dupuy & Liu (2012). For late-T dwarfs, the  $W2$  band has the smallest intrinsic scatter to the relation ( $\approx 0.19$  mag), so we use this band, even though its observed photometry has larger uncertainties than our near-IR photometry. We used a Monte Carlo calculation to account for the uncertainties in the spectral type (assumed to be uniformly distributed), the  $W2$  photometry (normally distributed), and the relation’s intrinsic scatter (normally distributed). The resulting distance modulus is  $4.08 \pm 0.28$  mag, corresponding to a distance of  $65_{-8}^{+9}$  pc. (The same calculation using  $J$  band gives a consistent result,  $55_{-10}^{+12}$  pc.)

Based on the photometric distance of  $\approx 65$  pc, the anticipated annual parallactic shift of  $\approx 15$  mas is well below the astrometric accuracy of our data. Moreover the UKIRT exposure and the NIRI

exposures were taken around the same time of year providing a six year baseline while further minimizing the parallactic shift. The proper motion of the source between these two exposures with respect to the field stars is  $-120 \pm 30$  mas/yr, and  $200 \pm 30$  mas/yr along the RA and DEC axes respectively. Further details of our NIR astrometry are given in Appendix B5. Combined with the measured proper motion and its uncertainties, the corresponding tangential velocity is  $73 \pm 14$  km s $^{-1}$ . This makes BDR 1750+3809 likely member of the thin disk population, based on the kinematic criteria in Dupuy & Liu (2012).

### 3. DISCUSSION

#### 3.1. Emission mechanism

Brown dwarf radio emission falls into two phenomenological categories: (a) impulsive highly polarized emission from the cyclotron maser instability (ECMI; Hallinan et al. 2007, 2008; Kao et al. 2018; Route & Wolszczan 2016a,b), and (b) quasi-quiet emission with low polarization fraction that is attributed to incoherent gyrosynchrotron emission (Berger et al. 2001; Williams et al. 2015; Osten et al. 2006). Adopting the photometric distance of  $d = 65$  pc, the brightness temperature of the emitter in BDR 1750+3809 is  $T_b \approx 10^{15} \text{ K } x_*^{-2}$ , where  $x_*$  is the radius of the emitter in units of the characteristic brown dwarf radius of  $7 \times 10^9$  cm. The high brightness temperature and circular fraction summarily rules out all incoherent emission mechanism. We therefore interpret the observed radio emission as ECMI.

#### 3.2. Radio energetics & temporal variation

Circularly polarized radio emission in BDs is driven by magnetospheric acceleration processes (Hallinan et al. 2008, 2015), whose luminosity need not be rigidly related to the NIR luminosity that is determined by surface temperature and atmospheric composition. As such, the first radio selected BD in a flux-limited survey is likely to be more radio-luminous than the NIR-selected population.

Adopting the photometric distance of  $d_{\text{pc}} = 65$ , the time-averaged (8-hr exposure) radio spectral luminosity in our 2018 detection is  $\approx 5 \times 10^{15} \text{ erg s}^{-1} \text{ Hz}^{-1}$ . For comparison, highly polarized radio emission from previous T-dwarfs have only been detected to have time-averaged spectral luminosities below  $\sim 10^{13} \text{ erg s}^{-1} \text{ Hz}^{-1}$  (Kao et al. 2018, 2019; Williams et al. 2013). However, the brightest short-duration pulses from T-dwarfs typically last tens of seconds and attain a spectral luminosity of  $\sim 10^{15} \text{ erg s}^{-1} \text{ Hz}^{-1}$  (Route & Wolszczan 2016a,b). Such values are comparable to the 8-hr averaged value for BDR 1750+3809.

To search for short radio bursts and any signature of rotation modulation, we extracted the radio light curve of BDR 1750+3809 from our 2018 detection at varying temporal cadences (Fig. 4). The light curves do not show a clear sign of periodicity and we see no evidence of intense short-duration bursts that could account for a significant fraction of the quasi-quiet radio luminosity. We also computed a windowed FFT of the curves, as well as a Lomb-Scargle periodogram (Fig. 5). Again, we did not detect an unambiguous signature of periodicity (more details are available in the Appendix).

#### 3.3. Special geometry or unusually luminous?

That large distance-scale to BDR 1750+3809 is unusual given that it is the first radio-selected BD in a flux-limited survey. We explore two scenarios that may give BDR 1750+3809 its unusually large time-averaged spectral luminosity. The scenarios also correspond to the two acceleration mechanisms that are known to operate in the Jovian magnetosphere and postulated to operate in



BD magnetospheres—breakdown of co-rotation between the plasma and the magnetic field (Nichols et al. 2012; Turnpenney et al. 2017), and a sub-Alfvénic interaction with an orbiting companion (Turnpenney et al. 2018; Saur et al. 2013).

*Co-rotation breakdown:* One possibility is that there is nothing particular about BDR 1750+3809 when compared to other radio-loud T-dwarfs and that its high time-averaged spectral luminosity is merely a result of a special viewing geometry.<sup>2</sup> Based on the reference case of solar system planetary radio emissions, auroral radio emission is expected to primarily occur at high magnetic latitudes (Zarka 1998). It is also expected to be beamed along the surface of a cone aligned with its axis parallel to the ambient magnetic field and a large opening angle (Zarka 1998; Melrose & Dulk 1982; Treumann 2006). In the hypothetical case of perfect axial symmetry, there will not be any rotation modulation of the observed emission. Real magnetospheres possess some azimuthal anomaly and/or a misalignment between the rotation and magnetic axes (Russell & Dougherty 2010). In the general case, the anomaly leads to a strong rotational modulation of the observed emission. The resulting emission typically appears pulsed and the pulse pattern repeats at the rotation period (see for e.g. Hallinan et al. 2007; Route & Wolszczan 2016b; Kao et al. 2016, 2018). However, in specific geometries (equator-on view for instance), the emission may be visible over most rotational phases.<sup>3</sup> This scenario may explain our non-detection of periodicity due to the absence of strong rotational modulation. In addition, the radio non-detection in one of the 2018 exposures could be the result of intrinsic variability expected in masers. For comparison, Jovian ECMI emission shows variability between epoch of factors of several (Zarka et al. 2004).

*Sub-Alfvénic interaction:* Alternatively, the electrodynamic engine in BDR 1750+3809 maybe particularly luminous as it is driven by interaction with a close-by and/or large companion. In this case, the radiation is only beamed towards the Earth during specific combinations of the orbital phases of the companion and the rotational phase of the primary, similar to the visibility of the Io-related Jovian emission. This beaming geometry could account for the non-detection 2018-12-14 LOFAR exposure.

The occurrence rate of planets around cold brown-dwarfs is currently not well constrained (He et al. 2017). Nevertheless, a rough constraint on the companion’s size may be obtained by scaling up the Jupiter-Io benchmark to meet the observed radio luminosity. Taking the emission bandwidth of BDR 1750+3809 to be 200 MHz for an estimate, the lower limit on the isotropic luminosity in the radio band is  $10^{24} \text{ erg s}^{-1}$ . The Jupiter-Io system generates an average radio power of  $\sim 10^{17} \text{ erg s}^{-1}$  (Zarka et al. 2004; Zarka 1998). Assuming that the radio emission from BDR 1750+3809 is beamed into a solid angle of 0.16 sr as is the case for Io-driven Jovian emission (Zarka et al. 2004), the observed emission is  $10^5$  times more luminous than the Jupiter-Io system. Assuming the same interaction Mach-number as Io’s interaction and the same geometric factors, the Poynting flux from the interaction scales as  $R_{\text{obs}}^2 v B^2$  (Zarka 2007; Saur et al. 2013; Turnpenney et al. 2018), where  $R$  is the effective radius of the companion,  $v$  is the relative velocity between the co-rotating magnetic field and the orbiting companion, and  $B$  is the magnetic field at the radius of the companion. If we adopt a rotation period for BDR 1750+3809 of 2 hours that is comparable to other radio-loud T-dwarfs (Kao et al. 2018), and a surface field strength of 0.1 kG and the same orbital distance as that of Io, the necessary power can be achieved if the companion presents an obstruction of radius

<sup>2</sup> In that case, we recommend the qualified ‘R’ be dropped from the name.

<sup>3</sup> See Hess & Zarka (2011); Pineda et al. (2017) for examples of radio signatures of rotational modulation.

$\approx 0.25 R_J$ . Because a dipolar field evolves with distance as  $d^{-3}$ , the term  $vB^2$  in the expression for radio power evolves steeply as  $d^{-5}$ . Hence, this scenario admits a wide range of companion sizes.

### 3.4. Outlook

The total power in the auroral current on BDR 1750+3809 can be further constrained by optical recombination-line observations. Taking the radio power to be 1% of the kinetic power in the auroral electrons Zarka (2007); Lamy et al. (2011) yields a total kinetic power of  $10^{26} \text{ ergs s}^{-1}$  which should be readily detectable in Balmer line emission for instance. In addition, a parallax measurement is necessary to secure a distance estimate. This is especially true since any close companion will contaminate the NIR flux of the object and produce erroneous photometric distance estimates.

The two scenarios presented above can be tested with radio data. If the companion driven emission is the true scenario, then continued radio monitoring should reveal signatures of periodicity at the orbital period of the companion. Such observation will, however, prove challenging due to the large inherent variation in maser luminosity. If on the other hand, the special geometric alignment scenario is correct, then a search for BDs in short exposure radio images made with existing LOFAR data must reveal a large underlying population of bursts from BDs that do not have a special geometric alignment with respect to the Earth.

We end by noting that the BDR 1750+3809 is not only the first radio selected BD, but the low frequency of observation means that the magnetic field at the emitter is comparable to that anticipated in gas-giant exoplanets (Yadav & Thorngren 2017; Cauley et al. 2019; Reiners & Christensen 2010). Our discovery therefore bodes well for radio detections of exoplanet magnetospheres.

## ACKNOWLEDGMENTS

JRC thanks the Nederlandse Organisatie voor Wetenschappelijk Onderzoek (NWO) for support via the Talent Programme Veni grant. The authors thank Prof. Gregg Hallinan for commenting on the manuscript. This paper is based on data obtained with the International LOFAR Telescope (obs. IDs 691360 and 658492 as part of the LoTSS survey and obs. ID 763257 awarded to proposal LC13\_021). LOFAR is the Low Frequency Array designed and constructed by ASTRON. It has observing, data processing, and data storage facilities in several countries, that are owned by various parties (each with their own funding sources), and that are collectively operated by the ILT foundation under a joint scientific policy. The ILT resources have benefitted from the following recent major funding sources: CNRS-INSU, Observatoire de Paris and Université d’Orléans, France; BMBF, MIWF-NRW, MPG, Germany; Science Foundation Ireland (SFI), Department of Business, Enterprise and Innovation (DBEI), Ireland; NWO, The Netherlands; The Science and Technology Facilities Council, UK. This research made use of the Dutch national e-infrastructure with support of the SURF Cooperative (e-infra 180169) and the LOFAR e-infra group. The Jülich LOFAR Long Term Archive and the German LOFAR network are both coordinated and operated by the Jülich Supercomputing Centre (JSC), and computing resources on the supercomputer JUWELS at JSC were provided by the Gauss Centre for Supercomputing e.V. (grant CHTB00) through the John von Neumann Institute for Computing (NIC). This research made use of the University of Hertfordshire high-performance computing facility and the LOFAR-UK computing facility located at the University of Hertfordshire and supported by STFC [ST/P000096/1], and of the Italian LOFAR IT computing infrastructure supported and operated by INAF, and by the Physics Department of Turin university (under an agreement with Consorzio Interuniversitario per la Fisica Spaziale) at the C3S Supercomputing Centre, Italy. The paper is based on observations obtained at the international Gemini Observatory (DDT proposal DT-2019B-014), a program of NSF’s NOIRLab, which is managed by the Association of Universities for Research in Astronomy (AURA) under a cooperative agreement with the National Science Foundation on behalf of the Gemini Observatory partnership: the National Science Foundation (United States), National Research Council (Canada), Agencia Nacional de Investigación y Desarrollo (Chile), Ministerio de Ciencia, Tecnología e Innovación (Argentina), Ministério da Ciência, Tecnologia, Inovações e Comunicações (Brazil), and Korea Astronomy and Space Science Institute (Republic of Korea). *Software:* `python3`, `numpy`, `scipy`, `astropy`, `matplotlib`. *Facilities:* LOFAR, Gemini-North, WISE, UKIRT, Hale telescope.

## REFERENCES

- |   |  |
|---|--|
| <p>Bastian, T. S., Dulk, G. A., &amp; Leblanc, Y. 2000, ApJ, 545, 1058, doi: <a href="https://doi.org/10.1086/317864">10.1086/317864</a></p> <p>Berger, E., Ball, S., Becker, K. M., et al. 2001, Nature, 410, 338.<br/><a href="https://arxiv.org/abs/astro-ph/0102301">https://arxiv.org/abs/astro-ph/0102301</a></p> <p>Burgasser, A. J., Geballe, T. R., Leggett, S. K., Kirkpatrick, J. D., &amp; Golimowski, D. A. 2006, ApJ, 637, 1067, doi: <a href="https://doi.org/10.1086/498563">10.1086/498563</a></p> | <p>Burningham, B., Hardcastle, M., Nichols, J. D., et al. 2016, MNRAS, 463, 2202, doi: <a href="https://doi.org/10.1093/mnras/stw2065">10.1093/mnras/stw2065</a></p> <p>Callingham, J. R., Vedantham, H. K., Pope, B. J. S., Shimwell, T. W., &amp; the LoTSS Team. 2019, Research Notes of the American Astronomical Society, 3, 37, doi: <a href="https://doi.org/10.3847/2515-5172/ab07c3">10.3847/2515-5172/ab07c3</a></p> |
|---|--|



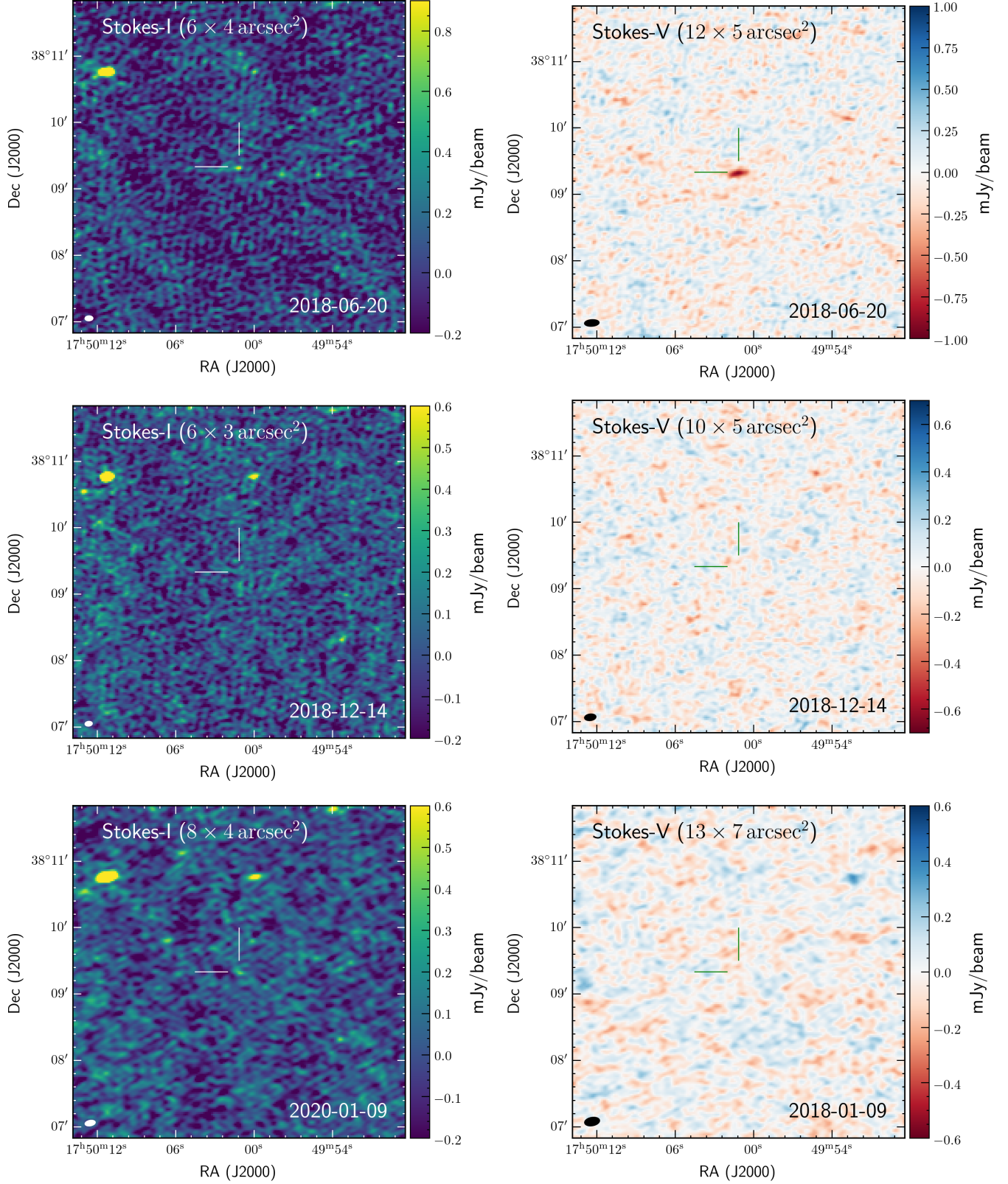


**Figure 1.** Radio detections and non-detections of BDR 1750+3809 with LOFAR. Left column shows Stokes-I (total intensity) images and right column shows Stokes-V (circularly polarized intensity) images made with Brigg's weighting with a factor of  $-0.5$  and  $0$  respectively. The observation dates and beam sizes are annotated. The position of BDR 1750+3809 is marked with cross-hairs that are  $30''$  long. The images are  $5'$  in size.

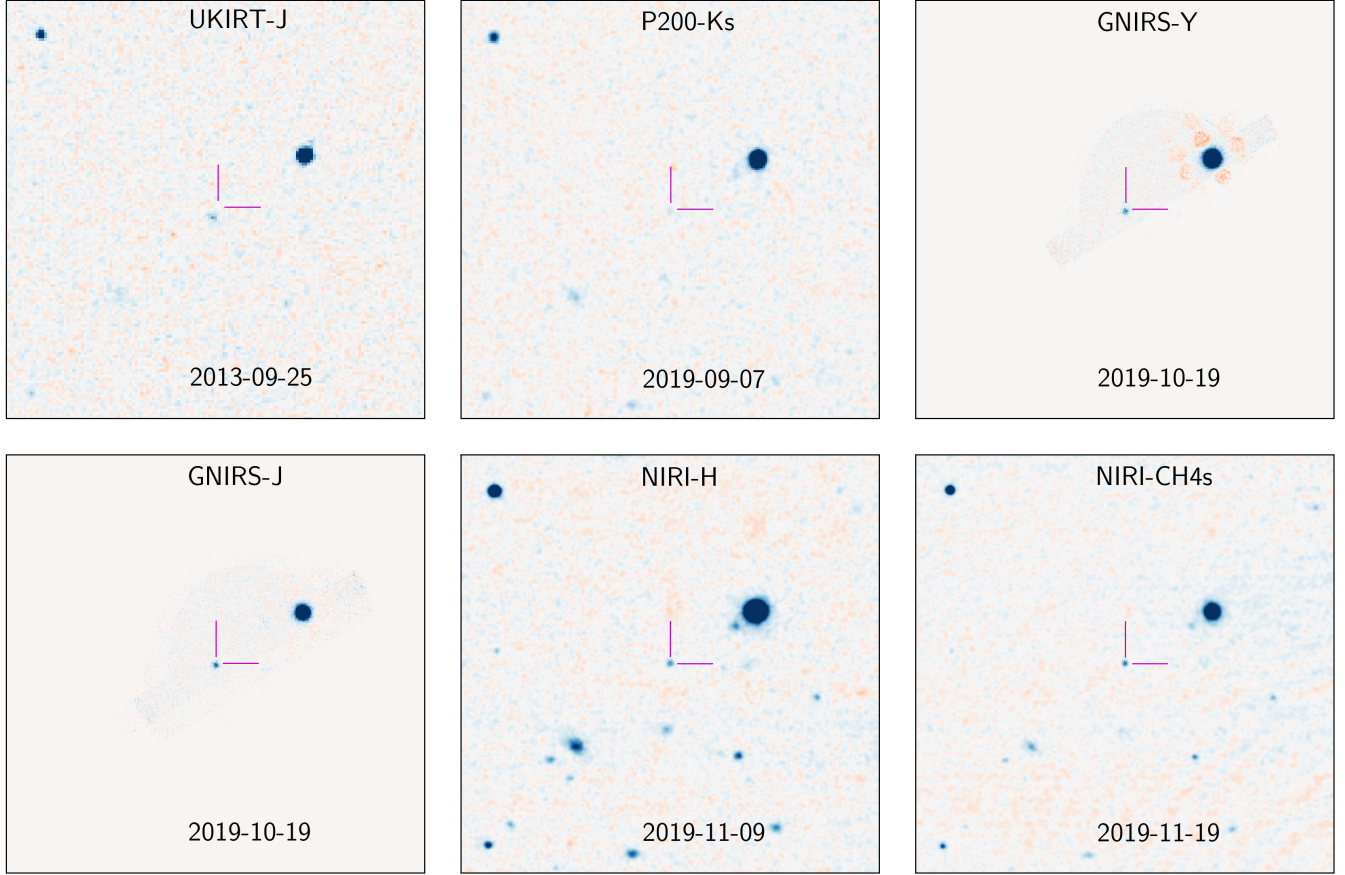


**Figure 2.** NIR images of the field around BDR 1750+3809. Because the images have disparate plate-scales, they have all been convolved with a Gaussian kernel with FWHM of  $0''.5$ . Instrument names, filters and observation dates are in the annotated text. The images are  $1'$  in size. The cross hairs are 5 arc-seconds long and point to the position of BDR 1750+3809 in the NIRI-CH4s exposure. Colour-scale runs from  $-25 \times \text{MAD}$  (red) to  $+25 \times \text{MAD}$  (blue), where MAD is the median absolute deviation and zero is denoted by white. Extracted source magnitudes and positions are given in Table 1. The roughly semicircular field of view of the GNIRS keyhole is smaller than the image dimension. The red circular patches in the GNIRS-Yband image are at the 1% level and are artifacts of flat-fielding.

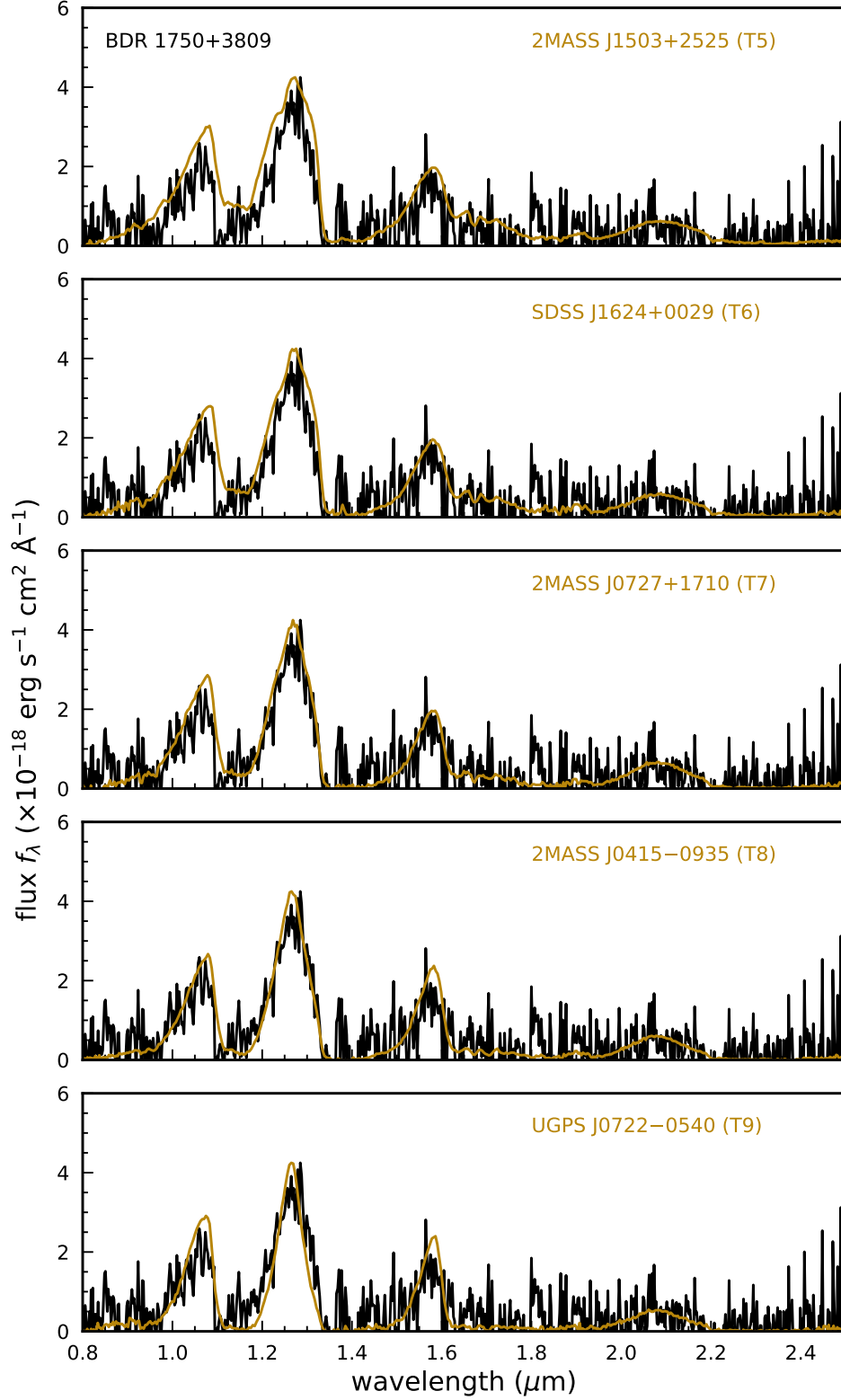


**Figure 3.** Near-IR spectrum of BDR1750+3809 (black) compared to T dwarf spectral standards (tan) from [Burgasser et al. \(2006\)](#) and [Cushing et al. \(2011\)](#). The spectra have been normalized by their peak flux.

Obs. date	Telescope / Instrument	Band	Flux density	Position
2013-09-25	UKIRT	$J$ -MK	$19^m.2(4)$	$17:50:01.18(2), +38:09:18.5(2)$
2018-06-20	LOFAR / HBA	144 MHz	$1.1(2) / -1.0(2)$ mJy	$17:50:01.15(5), 38:09:19.6(8)$
2018-12-14	LOFAR / HBA	144 MHz	$0.1(1) / -0.08(7)$ mJy	Non-detection
2020-01-09	LOFAR / HBA	144 MHz	$0.4(1) / -0.05(7)$ mJy	Marginal detection ( $4\sigma$ )
2019-09-07	Hale / WIRC	$K_s$	$19^m.2(4)$	Marginal detection ( $3\sigma$ )
2019-10-19	Gemini-N / GNIRS	$J$ -MK	$19^m.1(1)$	$17:50:01.13(2), +38:09:19.5(2)$
2019-10-19	Gemini-N / GNIRS	$Y$ -MK	$20^m.4(1)$	$17:50:01.12(2), +38:09:19.4(2)$
2019-11-09	Gemini-N / NIRC	$H$ -MK	$19^m.9(1)$	$17:50:01.13(2), +38:09:19.5(2)$
2019-11-13	Gemini-N / NIRC	$CH_4s$	$19^m.3(1)$	$17:50:01.12(2), +38:09:19.6(2)$
Various (co-add)	un-WISE	W1	$18^m.8(2)$	$17:50:01(1), +38:09:19.7(7)$
Various (co-add)	un-WISE	W2	$17^m.2(2)$	$17:50:01(1), +38:09:20.3(7)$

**Table 1.** Photometry and astrometry of BDR1750+3809 in J2000. Radio flux densities are given for Stokes-I and Stokes-V emission. Magnitudes are in the Vega system. Numbers in parenthesis give the error on the last significant digit. Errors in magnitude only include formal errors from aperture photometry and do not include systematic photometric errors (see appendix for further details).

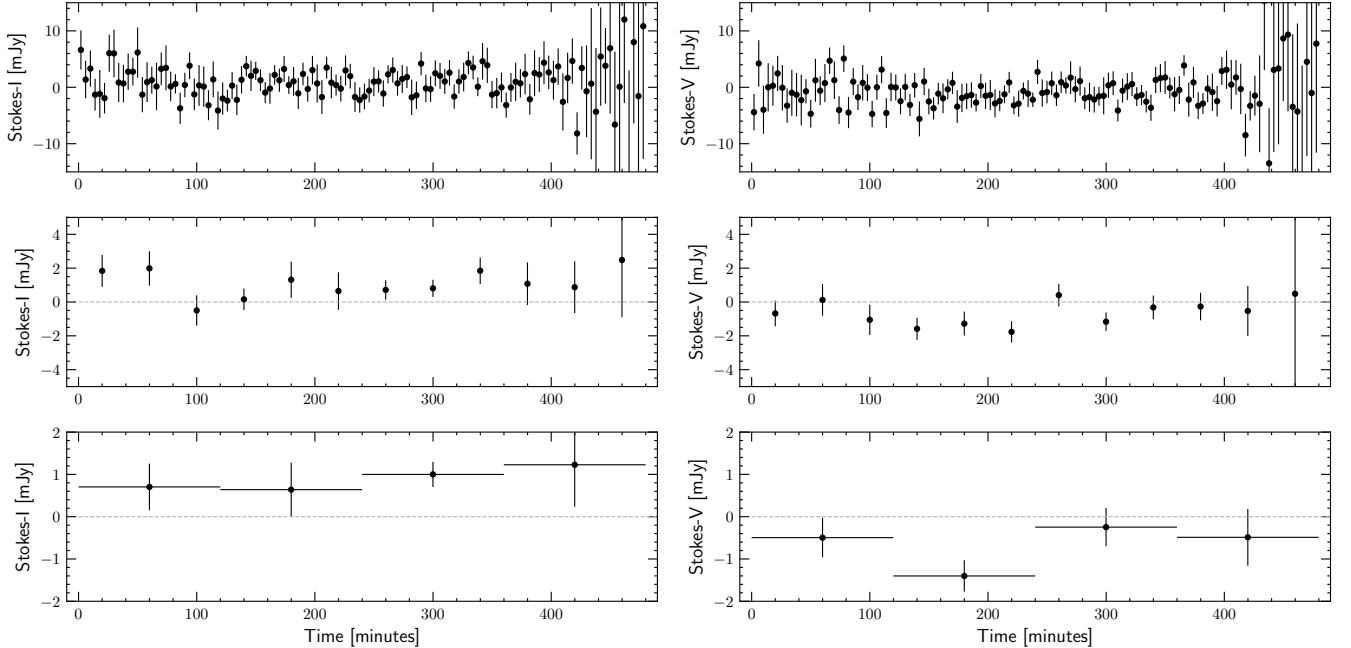


**Figure 4.** Stokes-I and Stokes-V light curves of BDR 1750+3809 (left and right hand columns) from the 2018 detection (see Fig. 1) at varying temporal resolutions of  $4^m$ ,  $40^m$ , and  $120^m$  (top to bottom). The light curves show that the emission has a stable brightness, with no obvious bright bursts.



- Callingham, J. R., Vedantham, H. K., Shimwell, T. W., & Pope, B. J. S. 2020, *Nature astronomy* (under review), xxx, xxx
- Cauley, P. W., Shkolnik, E. L., Llama, J., & Lanza, A. F. 2019, *Nature Astronomy*, 3, 1128, doi: [10.1038/s41550-019-0840-x](https://doi.org/10.1038/s41550-019-0840-x)
- Chambers, K. C., Magnier, E. A., Metcalfe, N., et al. 2016, arXiv e-prints, arXiv:1612.05560, <https://arxiv.org/abs/1612.05560>
- Christensen, U. R., Holzwarth, V., & Reiners, A. 2009, *Nature*, 457, 167, doi: [10.1038/nature07626](https://doi.org/10.1038/nature07626)
- Cushing, M. C., Vacca, W. D., & Rayner, J. T. 2004, *PASP*, 116, 362, doi: [10.1086/382907](https://doi.org/10.1086/382907)
- Cushing, M. C., Kirkpatrick, J. D., Gelino, C. R., et al. 2011, *ApJ*, 743, 50, doi: [10.1088/0004-637X/743/1/50](https://doi.org/10.1088/0004-637X/743/1/50)
- Cutri, R. M., & et al. 2013, *VizieR Online Data Catalog*, II/328
- De, K., Hankins, M. J., Kasliwal, M. M., et al. 2020, *PASP*, 132, 025001, doi: [10.1088/1538-3873/ab6069](https://doi.org/10.1088/1538-3873/ab6069)
- Deeg, H. J., & Belmonte, J. A. 2018, *Handbook of Exoplanets*, doi: [10.1007/978-3-319-55333-7](https://doi.org/10.1007/978-3-319-55333-7)
- Dupuy, T. J., & Liu, M. C. 2012, *ApJS*, 201, 19, doi: [10.1088/0067-0049/201/2/19](https://doi.org/10.1088/0067-0049/201/2/19)
- Dye, S., Lawrence, A., Read, M. A., et al. 2018, *MNRAS*, 473, 5113, doi: [10.1093/mnras/stx2622](https://doi.org/10.1093/mnras/stx2622)
- Elias, J. H., Joyce, R. R., Liang, M., et al. 2006, in *Society of Photo-Optical Instrumentation Engineers (SPIE) Conference Series*, Vol. 6269, Society of Photo-Optical Instrumentation Engineers (SPIE) Conference Series, 62694C, doi: [10.1117/12.671817](https://doi.org/10.1117/12.671817)
- Fegley, Bruce, J., & Lodders, K. 1996, *ApJL*, 472, L37, doi: [10.1086/310356](https://doi.org/10.1086/310356)
- Gaia Collaboration, Brown, A. G. A., Vallenari, A., et al. 2018, *A&A*, 616, A1, doi: [10.1051/0004-6361/201833051](https://doi.org/10.1051/0004-6361/201833051)
- Hallinan, G., Antonova, A., Doyle, J. G., et al. 2008, *ApJ*, 684, 644, doi: [10.1086/590360](https://doi.org/10.1086/590360)
- Hallinan, G., Sirothia, S. K., Antonova, A., et al. 2013, *ApJ*, 762, 34, doi: [10.1088/0004-637X/762/1/34](https://doi.org/10.1088/0004-637X/762/1/34)
- Hallinan, G., Bourke, S., Lane, C., et al. 2007, *ApJL*, 663, L25, doi: [10.1086/519790](https://doi.org/10.1086/519790)
- Hallinan, G., Littlefair, S. P., Cotter, G., et al. 2015, *Nature*, 523, 568, doi: [10.1038/nature14619](https://doi.org/10.1038/nature14619)
- Hancock, P. J., Murphy, T., Gaensler, B. M., Hopkins, A., & Curran, J. R. 2012, *MNRAS*, 422, 1812, doi: [10.1111/j.1365-2966.2012.20768.x](https://doi.org/10.1111/j.1365-2966.2012.20768.x)
- Hancock, P. J., Trott, C. M., & Hurley-Walker, N. 2018, *PASA*, 35, e011, doi: [10.1017/pasa.2018.3](https://doi.org/10.1017/pasa.2018.3)
- He, M. Y., Triaud, A. H. M. J., & Gillon, M. 2017, *MNRAS*, 464, 2687, doi: [10.1093/mnras/stw2391](https://doi.org/10.1093/mnras/stw2391)
- Hess, S. L. G., & Zarka, P. 2011, *A&A*, 531, A29, doi: [10.1051/0004-6361/201116510](https://doi.org/10.1051/0004-6361/201116510)
- Hodapp, K. W., Jensen, J. B., Irwin, E. M., et al. 2003, *PASP*, 115, 1388, doi: [10.1086/379669](https://doi.org/10.1086/379669)
- Kao, M. M., Hallinan, G., & Pineda, J. S. 2019, *MNRAS*, 487, 1994, doi: [10.1093/mnras/stz1372](https://doi.org/10.1093/mnras/stz1372)
- Kao, M. M., Hallinan, G., Pineda, J. S., et al. 2016, *ApJ*, 818, 24, doi: [10.3847/0004-637X/818/1/24](https://doi.org/10.3847/0004-637X/818/1/24)
- Kao, M. M., Hallinan, G., Pineda, J. S., Stevenson, D., & Burgasser, A. 2018, *ApJS*, 237, 25, doi: [10.3847/1538-4365/aac2d5](https://doi.org/10.3847/1538-4365/aac2d5)
- Kirkpatrick, J. D., Reid, I. N., Liebert, J., et al. 1999, *ApJ*, 519, 802, doi: [10.1086/307414](https://doi.org/10.1086/307414)
- Lacy, M., Baum, S. A., Chandler, C. J., et al. 2020, *PASP*, 132, 035001, doi: [10.1088/1538-3873/ab63eb](https://doi.org/10.1088/1538-3873/ab63eb)
- Lamy, L., Cecconi, B., Zarka, P., et al. 2011, *Journal of Geophysical Research (Space Physics)*, 116, A04212, doi: [10.1029/2010JA016195](https://doi.org/10.1029/2010JA016195)
- Lazio, T. Joseph, W., Farrell, W. M., Dietrick, J., et al. 2004, *ApJ*, 612, 511, doi: [10.1086/422449](https://doi.org/10.1086/422449)
- Leggett, S. K., Tremblin, P., Esplin, T. L., Luhman, K. L., & Morley, C. V. 2017, *ApJ*, 842, 118, doi: [10.3847/1538-4357/aa6fb5](https://doi.org/10.3847/1538-4357/aa6fb5)
- Lenc, E., Murphy, T., Lynch, C. R., Kaplan, D. L., & Zhang, S. N. 2018, *MNRAS*, 478, 2835, doi: [10.1093/mnras/sty1304](https://doi.org/10.1093/mnras/sty1304)
- Liu, M. C., Dupuy, T. J., & Ireland, M. J. 2008, *ApJ*, 689, 436, doi: [10.1086/591837](https://doi.org/10.1086/591837)
- Lynch, C. R., Lenc, E., Kaplan, D. L., Murphy, T., & Anderson, G. E. 2017a, *ApJL*, 836, L30, doi: [10.3847/2041-8213/aa5ffdf](https://doi.org/10.3847/2041-8213/aa5ffdf)
- Lynch, C. R., Murphy, T., Kaplan, D. L., Ireland, M., & Bell, M. E. 2017b, *MNRAS*, 467, 3447, doi: [10.1093/mnras/stx354](https://doi.org/10.1093/mnras/stx354)
- Melrose, D. B., & Dulk, G. A. 1982, *ApJ*, 259, 844, doi: [10.1086/160219](https://doi.org/10.1086/160219)
- Nakajima, T., Tsuji, T., & Yanagisawa, K. 2004, *ApJ*, 607, 499, doi: [10.1086/383299](https://doi.org/10.1086/383299)



- Nichols, J. D., Burleigh, M. R., Casewell, S. L., et al. 2012, *ApJ*, 760, 59, doi: [10.1088/0004-637X/760/1/59](https://doi.org/10.1088/0004-637X/760/1/59)
- Osten, R. A., Hawley, S. L., Bastian, T. S., & Reid, I. N. 2006, *ApJ*, 637, 518, doi: [10.1086/498345](https://doi.org/10.1086/498345)
- Pineda, J. S., Hallinan, G., & Kao, M. M. 2017, *ApJ*, 846, 75, doi: [10.3847/1538-4357/aa8596](https://doi.org/10.3847/1538-4357/aa8596)
- Rayner, J. T., Toomey, D. W., Onaka, P. M., et al. 2003, *PASP*, 115, 362
- Reiners, A., & Christensen, U. R. 2010, *A&A*, 522, A13, doi: [10.1051/0004-6361/201014251](https://doi.org/10.1051/0004-6361/201014251)
- Rosenthal, E. D., Gurwell, M. A., & Ho, P. T. P. 1996, *Nature*, 384, 243, doi: [10.1038/384243a0](https://doi.org/10.1038/384243a0)
- Route, M., & Wolszczan, A. 2016a, *ApJ*, 830, 85, doi: [10.3847/0004-637X/830/2/85](https://doi.org/10.3847/0004-637X/830/2/85)
- . 2016b, *ApJL*, 821, L21, doi: [10.3847/2041-8205/821/2/L21](https://doi.org/10.3847/2041-8205/821/2/L21)
- Russell, C. T., & Dougherty, M. K. 2010, *SSRv*, 152, 251, doi: [10.1007/s11214-009-9621-7](https://doi.org/10.1007/s11214-009-9621-7)
- Saur, J., Grambusch, T., Duling, S., Neubauer, F. M., & Simon, S. 2013, *A&A*, 552, A119, doi: [10.1051/0004-6361/201118179](https://doi.org/10.1051/0004-6361/201118179)
- Schlafly, E. F., Meisner, A. M., & Green, G. M. 2019, *ApJS*, 240, 30, doi: [10.3847/1538-4365/aafbea](https://doi.org/10.3847/1538-4365/aafbea)
- Schrijver, C. J., & Zwaan, C. 2008, *Solar and Stellar Magnetic Activity* (Cambridge University Press)
- Schwenn, R. 2006, *Living Reviews in Solar Physics*, 3, 2, doi: [10.12942/lrsp-2006-2](https://doi.org/10.12942/lrsp-2006-2)
- Shimwell, T. W., Röttgering, H. J. A., Best, P. N., et al. 2017, *A&A*, 598, A104, doi: [10.1051/0004-6361/201629313](https://doi.org/10.1051/0004-6361/201629313)
- Shimwell, T. W., Tasse, C., Hardcastle, M. J., et al. 2019, *A&A*, 622, A1, doi: [10.1051/0004-6361/201833559](https://doi.org/10.1051/0004-6361/201833559)
- Skrutskie, M. F., Cutri, R. M., Stiening, R., et al. 2006, *AJ*, 131, 1163, doi: [10.1086/498708](https://doi.org/10.1086/498708)
- Stephens, D. C., & Leggett, S. K. 2004, *PASP*, 116, 9, doi: [10.1086/381135](https://doi.org/10.1086/381135)
- Tinney, C. G., Burgasser, A. J., Kirkpatrick, J. D., & McElwain, M. W. 2005, *AJ*, 130, 2326, doi: [10.1086/491734](https://doi.org/10.1086/491734)
- Treumann, R. A. 2006, *A&A Rv*, 13, 229, doi: [10.1007/s00159-006-0001-y](https://doi.org/10.1007/s00159-006-0001-y)
- Turnpenney, S., Nichols, J. D., Wynn, G. A., & Burleigh, M. R. 2018, *ApJ*, 854, 72, doi: [10.3847/1538-4357/aaa59c](https://doi.org/10.3847/1538-4357/aaa59c)
- Turnpenney, S., Nichols, J. D., Wynn, G. A., & Casewell, S. L. 2017, *MNRAS*, 470, 4274, doi: [10.1093/mnras/stx1508](https://doi.org/10.1093/mnras/stx1508)
- Vacca, W. D., Cushing, M. C., & Rayner, J. T. 2003, *PASP*, 115, 389
- van Haarlem, M. P., Wise, M. W., Gunst, A. W., et al. 2013, *A&A*, 556, A2, doi: [10.1051/0004-6361/201220873](https://doi.org/10.1051/0004-6361/201220873)
- Vedantham, H. K., Callingham, J. R., Shimwell, T. W., et al. 2020, *Nature Astronomy*, 4, 577, doi: [10.1038/s41550-020-1011-9](https://doi.org/10.1038/s41550-020-1011-9)
- Williams, P. K. G. 2018, *Radio Emission from Ultracool Dwarfs* (Springer International Publishing), 171, doi: [10.1007/978-3-319-55333-7\\_171](https://doi.org/10.1007/978-3-319-55333-7_171)
- Williams, P. K. G., Berger, E., & Zauderer, B. A. 2013, *ApJL*, 767, L30, doi: [10.1088/2041-8205/767/2/L30](https://doi.org/10.1088/2041-8205/767/2/L30)
- Williams, P. K. G., Casewell, S. L., Stark, C. R., et al. 2015, *ApJ*, 815, 64, doi: [10.1088/0004-637X/815/1/64](https://doi.org/10.1088/0004-637X/815/1/64)
- Wilson, J. C., Eikenberry, S. S., Henderson, C. P., et al. 2003, in *Society of Photo-Optical Instrumentation Engineers (SPIE) Conference Series*, Vol. 4841, Instrument Design and Performance for Optical/Infrared Ground-based Telescopes, ed. M. Iye & A. F. M. Moorwood, 451–458, doi: [10.1117/12.460336](https://doi.org/10.1117/12.460336)
- Wu, C. S., & Lee, L. C. 1979, *ApJ*, 230, 621, doi: [10.1086/157120](https://doi.org/10.1086/157120)
- Yadav, R. K., & Thorngren, D. P. 2017, *ApJL*, 849, L12, doi: [10.3847/2041-8213/aa93fd](https://doi.org/10.3847/2041-8213/aa93fd)
- Zarka, P. 1998, *J. Geophys. Res.*, 103, 20159, doi: [10.1029/98JE01323](https://doi.org/10.1029/98JE01323)
- . 2007, *Planet. Space Sci.*, 55, 598, doi: [10.1016/j.pss.2006.05.045](https://doi.org/10.1016/j.pss.2006.05.045)
- Zarka, P., Cecconi, B., & Kurth, W. S. 2004, *Journal of Geophysical Research (Space Physics)*, 109, A09S15, doi: [10.1029/2003JA010260](https://doi.org/10.1029/2003JA010260)

## APPENDIX

## A. RADIO DATA

A.1. *Data reduction*

We used the standard LoTSS pipeline for primary data reduction (Shimwell et al. 2017, 2019). An additional self-calibration step was applied in the direction of the target with a pipeline that is described in Vedantham et al. (2020). All images were made with `wsclean` with Briggs’s weighting. The images in Fig. 1 have a weighting factor of  $-0.5$  for Stokes-I to suppress confusion from diffuse emission and sidelobe noise. The Stokes-V images do not suffer from these sources of confusion and have been made with a weighting factor of  $0$  to maximize signal to noise ratio. The astrometric fits and flux density in Table 1 were determined from images made with a weighting factor of  $-0.5$  to improve astrometric accuracy.

We used the Background And Noise Estimator (BANE) and source finder AEGEAN (v 2.1.1; Hancock et al. 2012, 2018) to measure the flux density and location of BDR 1750+3809. Originally, we discovered BDR 1750+3809 through a blind search for sources that were  $> 4\sigma$  in Stokes V emission, where  $\sigma$  is the local rms noise (Callingham et al. 2019; Vedantham et al. 2020). Once the position of the source was known, we applied the prioritised fitting option of AEGEAN for the other epochs, which fits for both the PSF shape and flux density of BDR 1750+3809. In the Stokes V images we searched for both positive and negative emission.

The right source to the NE of the target has a peak Stokes-I flux density of  $\sim 8.5$  mJy and is undetected in the Stokes-V images with rms noise of  $0.1$  mJy, suggesting that the Stokes I to V leakage is at the  $\sim 1\%$  level of below in our images.

A.2. *Light curves*

Although the 8-hr exposure images have good  $uv$  coverage, the short exposures suffer from sidelobe noise from in-field sources. We therefore modelled the visibilities of the in-field sources using the `update-model-column` option of `wsclean` and subtracted the model from the visibilities. To extract the light curves at the location of BDR 1750+3809, the residual visibilities were then snapshot imaged at varying temporal cadences of with a Briggs’s factor of  $0$ .

A.3. *Radio astrometry*

The LoTSS astrometry is tied to the Pan-STARRS grid with an absolute astrometric error of  $0''.2$  (Shimwell et al. 2017, 2019). In Table 1 we quote the error obtained by adding the formal error from our source finding in quadrature with the absolute astrometric error. Because BDR 1750+3809 is a faint source, its astrometric uncertainty in the radio is dominated by the formal error in finding the source centroid within the point spread function. For instance, the images used for astrometric determination from the 2018-06-20 exposure (Briggs’s factor of  $-0.5$ ) has a point spread function with major and minor axes of  $4'' \times 7''$ . Adopting a geometric mean width of  $5''.3$ , the formal centroid-finding error for a  $7\sigma$  source is  $0''.76$ .

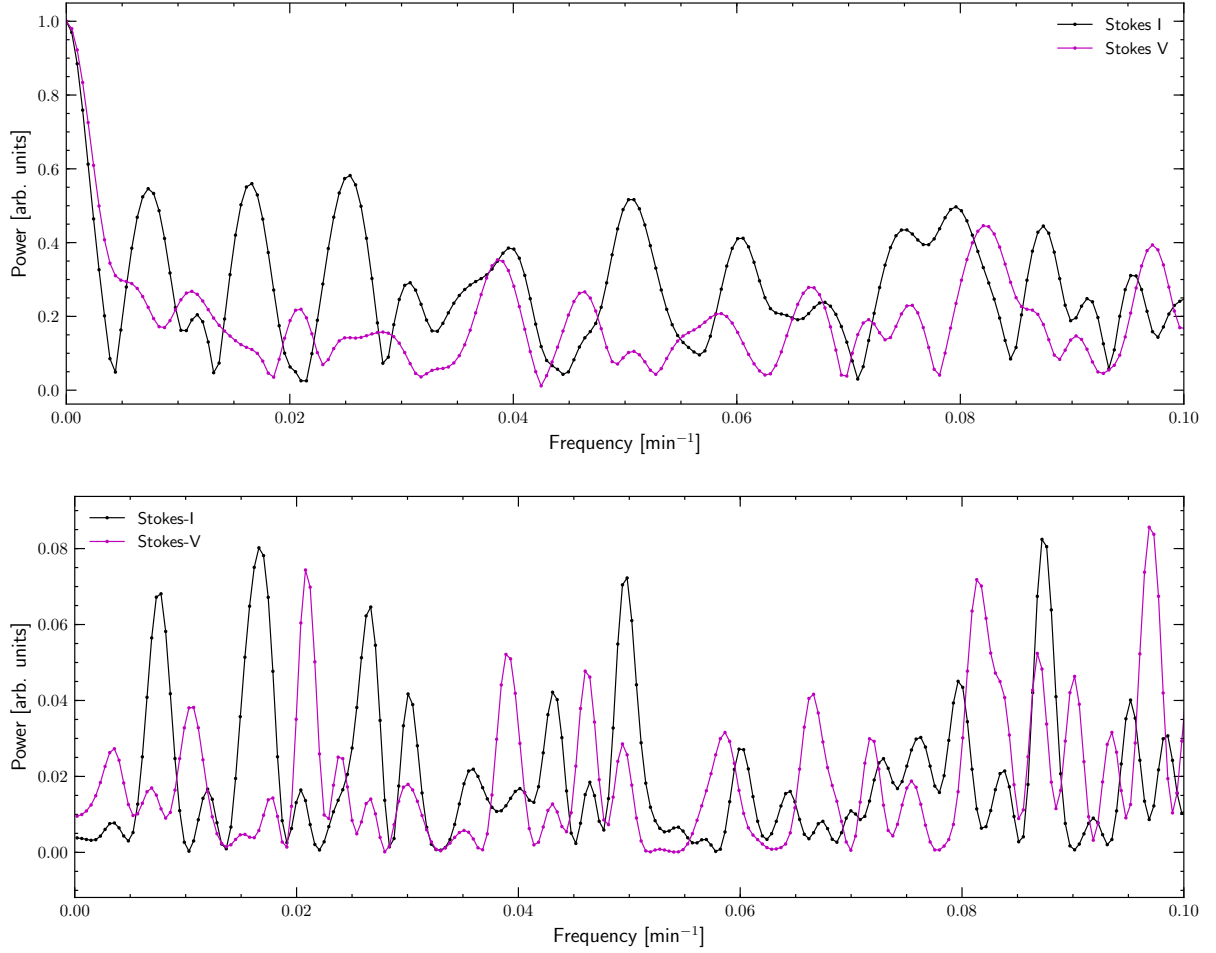


**Figure 5.** Power spectrum of temporal variations (top panel) and Lomb-Scargle periodogram (bottom panel). Light-curves at a 4 min cadence were used as input. A Hanning window was used to improve the point spread function of the FFT.

## B. NIR DATA REDUCTION

### B.1. *GNIRS* keyhole imaging

There was light cloud cover and fog during the observations. Dark and bias current was subtracted from each exposure using custom python code applied to calibration images taken at the end of the night. The dome-flat frames were unusable due to improper illumination (cause unknown), hence we used the median combination of the dithered science exposures to make a sky-flat. The pixel centroid of Star A in each frame was determined using `sExtractor`. The FITS header keywords `CRVAL1`, `CRPIX1`, `CRVAL2`, `CRPIX2` were modified to shift the frame so as to have Star A’s position tied to its *Gaia* DR2 position (Gaia Collaboration et al. 2018). The plate scale and orientation could not be solved for with just one reference star, so we adopted the nominal values specified by the observatory. The resulting frames were resampled on to a common grid and median-combined using the `swarp` software.

### B.2. *NIR imaging*

As with the GNIRS exposures, the observing conditions did not allow for photometric calibration transfer from standard stars. The dark and bias currents were subtracted from each exposure using custom python code. The dome flats were found to be inadequate. So we used the dithered science exposures to construct a sky-flat which was applied in addition to the dome-flats. For each exposure, we then used `sextractor` to extract sources and `scamp` to solve for plate distortions up to third order while using the USNO-B1 catalog as reference. Finally, we used `swarp` to re-sample the exposures on a common grid and median combine them.

### B.3. *NIR photometry*

Star A (2MASS J17500008+3809276) with a 2MASS *J*-band magnitude of  $15^{\text{m}}.22$  has measured flux densities in several optical, NIR and MIR bands (Fig. 6). From a smooth polynomial fit to the star's flux densities (in Jansky units) measured by the Pan-STARRS and 2MASS surveys, we estimated the Vega magnitude of Star A in the MKO-systems *Y*, *J*, *H* and  $\text{CH}_4\text{s}$  filters to be, respectively,  $15^{\text{m}}.78$ ,  $15^{\text{m}}.16$ ,  $14^{\text{m}}.58$  and  $14^{\text{m}}.61$ . In doing so we assumed the zero-points of 2026 Jy, 1545 Jy, 1030 Jy and 1071 Jy respectively. The fractional deviation of the Star A's photometric measurements in the near-infrared and the fit is within 1%, which is smaller than the final photometric uncertainty (see below). Based on its spectrum, the star is likely a mid M-dwarf (M3 or M4) which is not expected to have large spectral excursions in the NIR part of its spectrum. We checked individual exposures to make sure that the star did not display egregious flaring that would significantly affect its flux density in co-added images. To determine the flux density (in ADC counts), we first computed the growth curve of 2MASS stars in the field by measuring their flux in varying apertures. The growth curves were averaged to yield the average growth curve. The small field of view of the GNIRS keyhole exposures meant that the only available 2MASS star in the field was Star A. We then measured the flux of the target in different apertures—1.0, 1.25, 1.5 and so on until 2.5 times the FWHM of point spread function. To determine the targets total flux, we fit the average growth curve to the target's growth curve measured with these apertures. We took the mean value of the fitted fluxes as the measured target flux and their dispersion as the formal flux density fitting error. The target and Star A's flux densities (in counts) were finally scaled to match Star A's measured flux with its model SED (Fig. 6).

The formal flux fitting errors were  $0^{\text{m}}.02 - 0^{\text{m}}.05$  depending on the filter. We repeated the same photometric procedure on in-field 2MASS stars in our *H*-band and found our estimates to be differ from 2MASS estimates by about  $0^{\text{m}}.1$ . We therefore conservatively adopted this value as the final error in our photometry.

Given the marginal detection in the *K*s band image the aperture flux with radii much larger than the seeing FWHM were severely affected by background estimation errors. We therefore measured the flux only in a single aperture whose radius was comparable to the seeing FWHM, instead of fitting the growth curves at various apertures. The photometry was referred to Star A as in the case of the Gemini observations. We note that a filter correction of  $\approx -0^{\text{m}}.2$  for a late T-dwarf (Stephens & Leggett 2004), places the *K* band magnitude of BDR 1750+3809 in the MKO system at  $19^{\text{m}}.4(4)$ .

### B.4. *NIR spectroscopy*

We used the facility near-IR spectrograph Spex (Rayner et al. 2003) in prism mode, obtaining  $0.8\text{--}2.5\ \mu\text{m}$  spectra in a single order, with the  $0.8''$  wide slit oriented at the parallactic angle. To

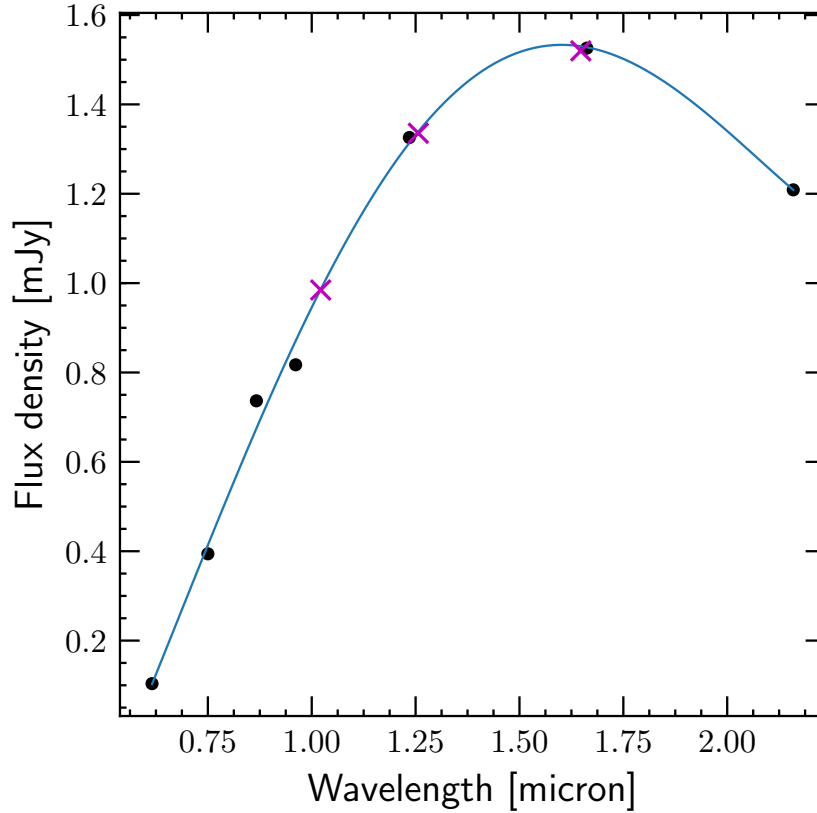


**Figure 6.** Measured (black dots) and estimated (magenta crosses) flux density of Star A (2MASS J17500008+3809276). The estimates are based on a smooth polynomial fit (solid blue line) to the measurements.

acquire BDR 1750+3809, we offset from Star A ( $J = 15.2$  mag) that lies  $14''$  WNW (offsets of  $12.25''$  east and  $7.19''$  south from the 2MASS star). BDR 1750+3809 was nodded along the slit in an ABBA pattern, with individual exposure times of 180 sec, and observed over an airmass range of 1.3–2.0, resulting in a total on-source exposure time of 4320 sec. The telescope was guided using the off-axis optical guide camera. We observed the A0 V star HD 165029 contemporaneously for flux and telluric calibration, interleaving observations of the science target and calibrator to minimize the airmass difference between the two. The spectra were reduced using version 4.1 of the SpeXtool software package (Vacca et al. 2003; Cushing et al. 2004).

#### B.5. *unWISE* detection

The original AllWISE catalogue does not have a source plausibly associated with BDR 1750+3809 even when accounting for proper motion. This catalogue had deliberately blurred point-spread function in the final co-added images. Recently Schlafly et al. (2019) have published ‘un-blurred’ co-added images and extracted catalog. The W2-filter image is shown in Fig. 7 and we have reported the catalog flux in Table 1. The catalog reports a detection of BDR 1750+3809, at the  $\approx 5\sigma$  level. It is flagged for the possible contamination from the wings of the bright source Star A to the North-West. Although there is almost of a decade that has elapsed within the exposures, the WISE point-spread function of  $6''.7$  is large enough for the proper-motion to not affect the flux determination significantly.



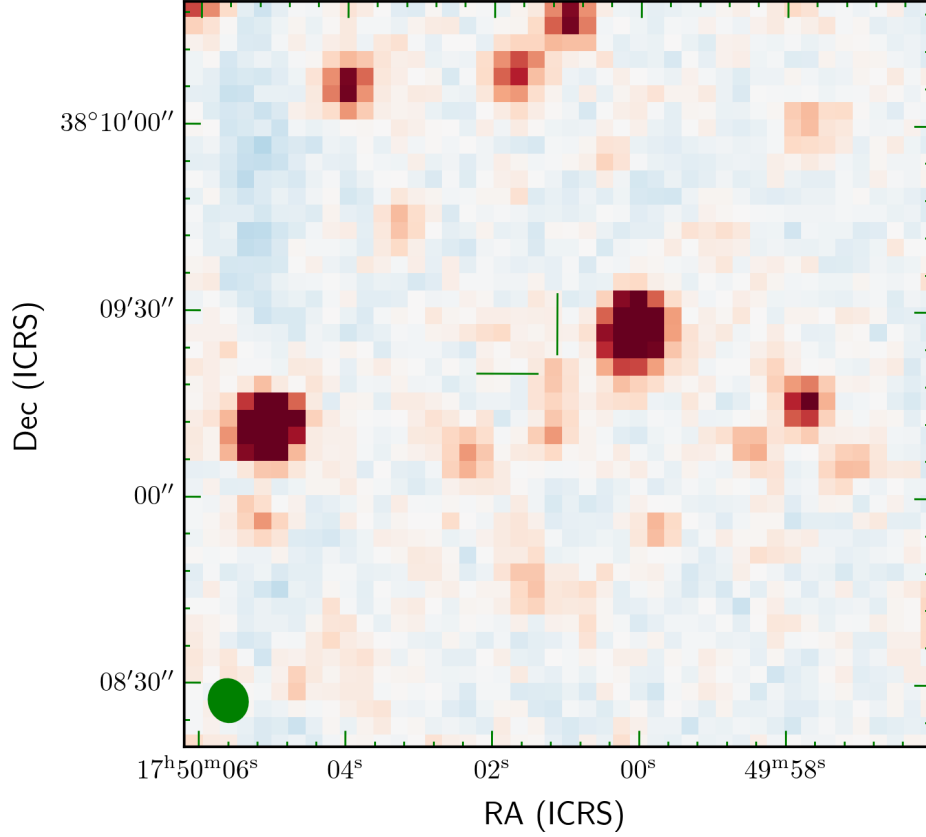


**Figure 7.** Image of the region around BDR 1750+3809 from the unWISE co-addition of WISE frames in filter W2 (centered on 4.5 microns). The plate-scale is  $2''.75$  and the beam is shown as a green ellipse. The yellow cross-hairs are  $10''$  in length and mark the position of BDR 1750+3809 from the NIRI-CH4s exposure (see table 1 and Fig. 2). Colorscale runs from -15 to 15 median absolute deviation.

#### B.6. NIR astrometry and proper motion

The GNIRS keyhole images only had the target and Star A detected within the field of view. We used Star A to apply a global offset and used the nominal plate scale and keyhole position angle to determine the position of BDR 1750+3809. The uncertainties on the plate scale and position angle are not well determined but are likely about 1% and  $0''.01$  respectively (priv. comm. Siyi Xu). Based on this, we conservatively adopt an uncertainty of  $0''.2$  in BDR 1750+3809’s position derived from GNIRS keyhole images.

The NIRI images allowed us to solve for offsets and distortions as many stars were detected. The exposures were set to the USNO-B1 astrometric frame. A final offset correction on the extracted position of BDR 1750+3809 was applied such that the median offset of field stars in the *gaia* DR2 catalog was zero. We checked the `sextractor` extracted positions of other in-field stars that were comparable in brightness to Star A and found the astrometric accuracy to be about  $0''.2$  which is likely dominated by uncertainties in our solution for plate scale and distortion terms. We note that the NIRI and GNIRS positions agree within errors.

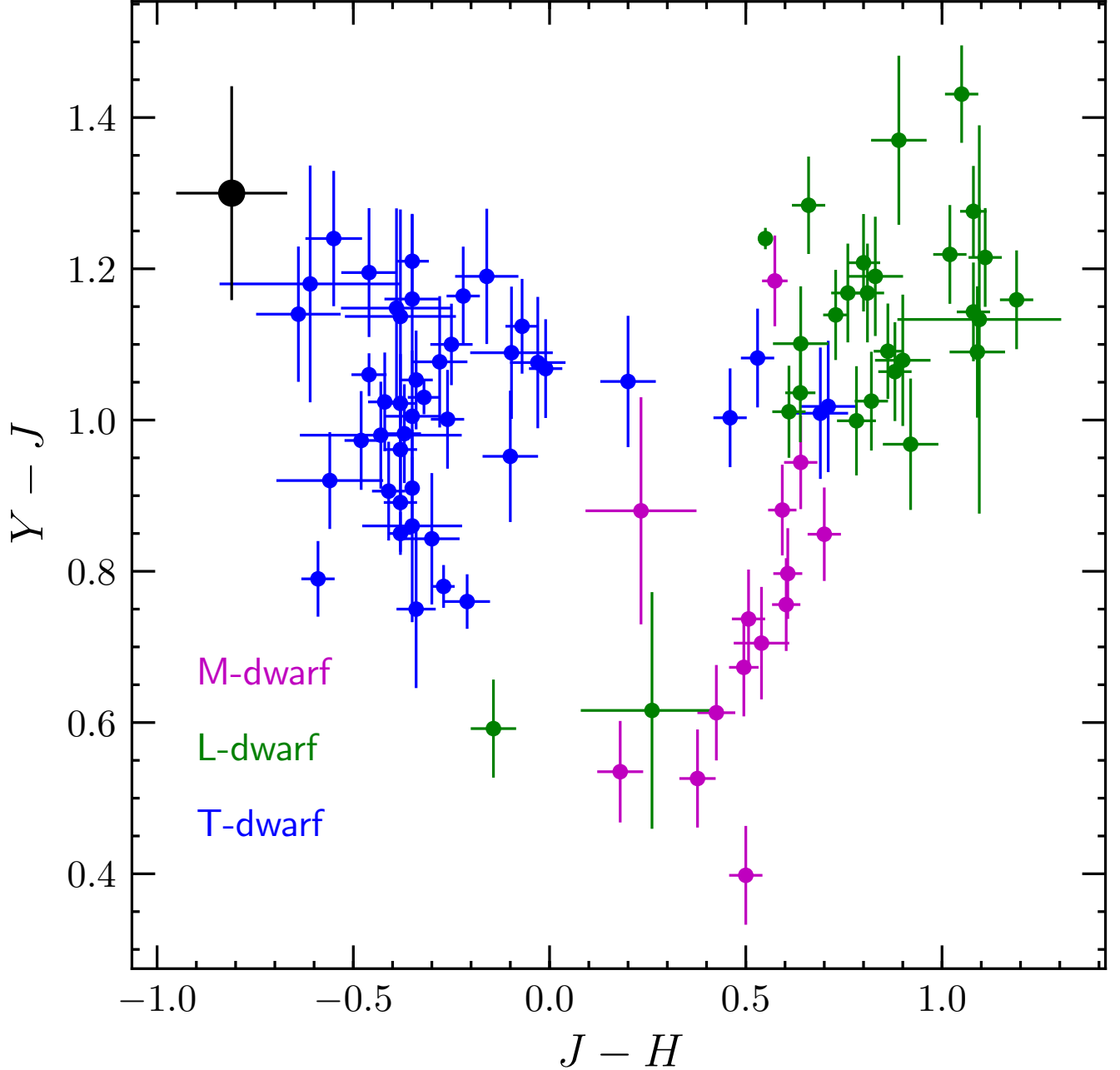


**Figure 8.** NIR colors of BDR 1750+3809 (shown in black) overplotted on the colours of M-, L- and T-dwarfs in the catalogue of Dupuy & Liu (2012). The colors demonstrate that BDR 1750+3809 is a T-dwarf.

We determined the proper motion of BDR 1750+3809, using the UKIRT and NIRI  $\text{CH}_4$ s exposures because the NIRI  $H$ -band exposure had worse seeing. Fig. 10 shows the offset of field stars and BDR 1750+3809 between the two images.

The apparent proper motion between the UKIRT exposure and the NIRI exposures is  $-120$  mas/yr, and  $200$  mas/yr along the RA and DEC axes respectively. Based on our astrometric accuracy, we estimate the error in these estimates to be about  $30$  mas/yr. We do not have sufficient number of measurements to simultaneously solve for parallax, proper motion and any orbital shift due to binarity.

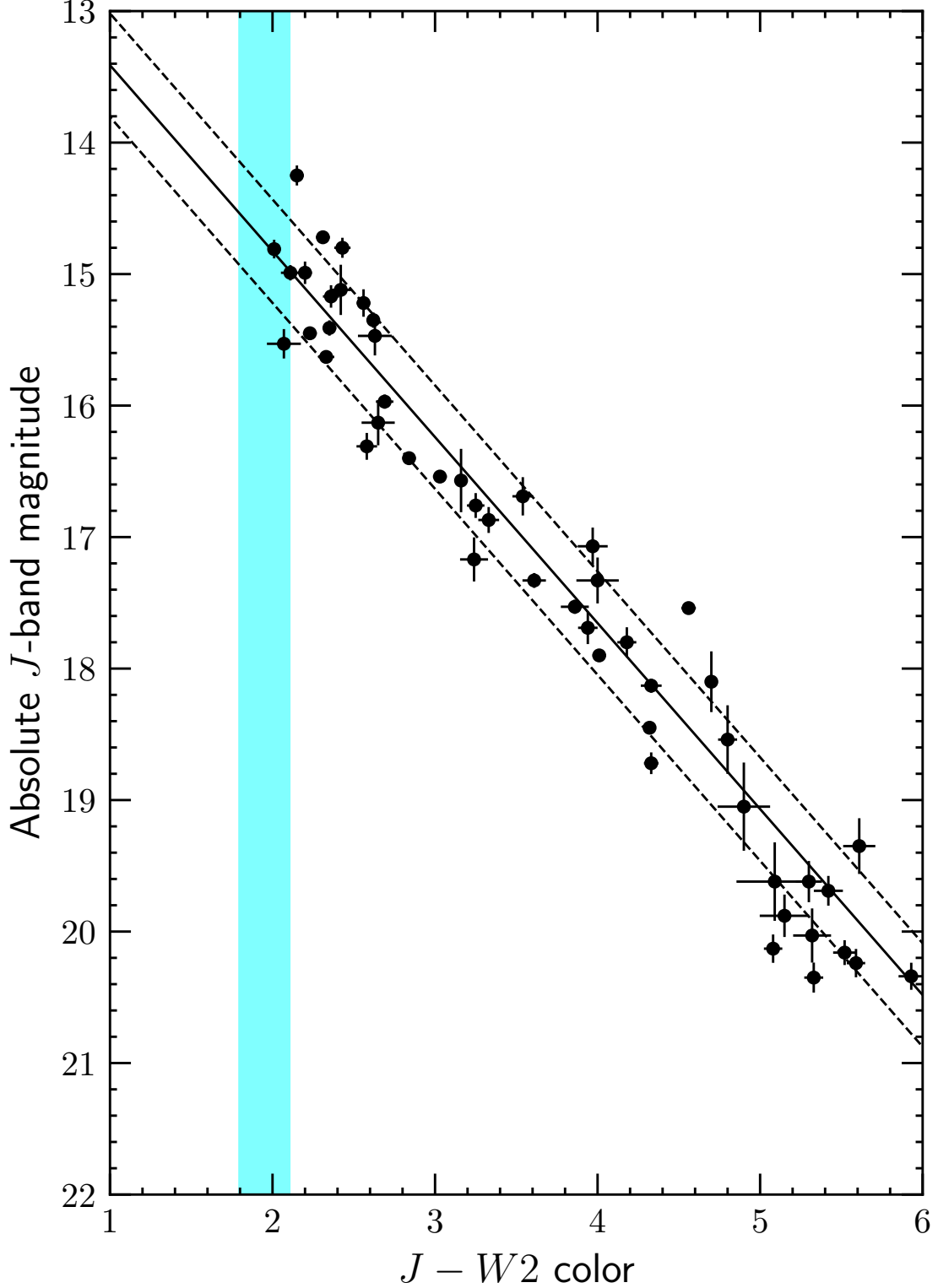


**Figure 9.** NIR color-magnitude diagram for cold brown dwarfs (class T and Y). Black points are taken from the homogenized dataset on late T-dwarfs and Y dwarfs presented by [Leggett et al. \(2017\)](#). The solid black line is a linear fit to the points. The dashed black lines are parallel to the solid line, and are offset by one standard deviation between the fit and the data points. The cyan shaded region shows the constraint on BDR 1750+3809’s NIR colors from Table 1

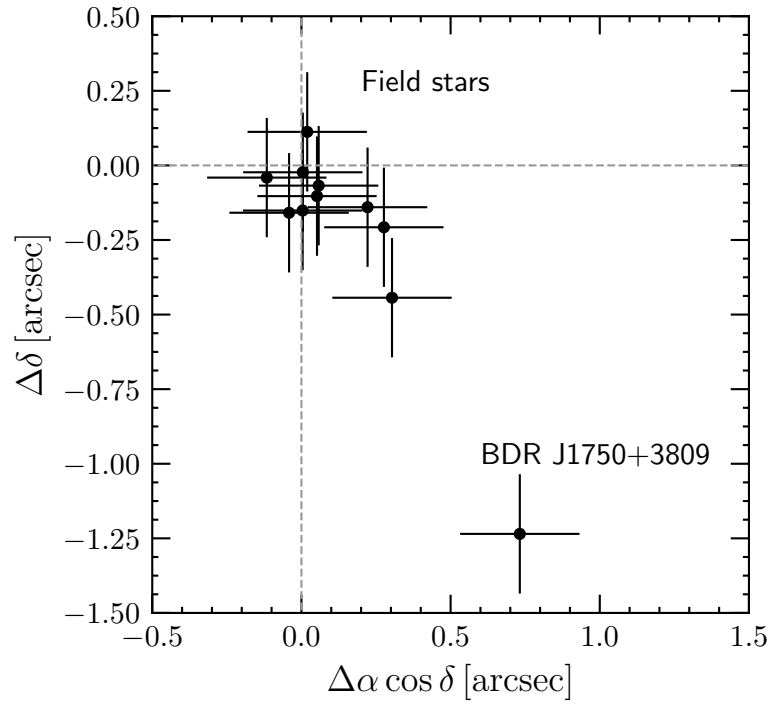


**Figure 10.** Astrometric offset of field stars and BDR 1750+3809 between the UKIRT and NIRI exposures, separated by about six years.